ADVANCED SENSOR RESEARCH Open Access
www.advsensorres.com

High-Resolution Printed Ethylene Vinyl Acetate Based Strain Sensor for Impact Sensing

Pariya Nazari, Johannes Zimmermann, Christian Melzer, Wolfgang Kowalsky, Jasmin Aghassi-Hagmann, Gerardo Hernandez-Sosa, and Uli Lemmer**

The strongly growing interest in digitalizing society requires simple and reliable strain-sensing concepts. In this work, a highly sensitive stretchable sensor is presented using a straightforward and scalable printing method. The piezoresistive sensor consists of conductive core–shell microspheres embedded in an elastomer. As the elastomer, ethylene vinyl acetate (EVA) is employed as an efficient and cost-effective alternative compared to polydimethylsiloxane (PDMS). EVA allows for a significantly lower percolation threshold and low hysteresis compared with PDMS. Using 35 µm microspheres, a detection limit of 0.01% is achieved. When using 4 µm microspheres, the sensor shows a detection limit of 0.015% and electromechanical robustness against 1000 cycles of 0–1% strain. The stretchable strain sensor is successfully implemented as an impact sensor and a diaphragm expansion monitoring sensor. Fast (20 ms) and high-resolution response as well as mechanical robustness to strain values greater than the linear working range of the sensor are demonstrated. The results of this research indicate the promising potential of employing conductive microspheres embedded in the EVA matrix for fast and precise strain detection applications.

1. Introduction

Small and stretchable strain sensors have various potential applications in the future of digital society such as workplace safety in factories, health care, soft robotics, or immersive gaming experiences, all of which contribute to an enhanced quality of life.[1] This ever-growing interest in conformable electronics requires not only scalable and cost-effective fabrication methods but also high-resolution sensors with reasonable stretchability. Among the various sensing concepts in stretchable sensors presented so far, a printed composite of stretchable polymer housing conductive particles offers a simple sensing mechanism and one of the most cost-effective fabrication possibilities.[2] In these materials, conductive paths begin to form at a critical volume ratio between the conductive filler and the elastomer, i.e., the percolation threshold.[3] The main sensing principle of such sensors is piezoresistivity, i.e., the change in electrical resistance upon an externally applied mechanical deformation, e.g. tensile strain (ϵ). The performance characteristics of the composite sensor (e.g., the minimum strain that can be detected) are determined by how the chosen elastomer, the conductive constituents, and the interface between the two interact under strain. For most applications, high sensitivity (i.e., an easily detectable signal when a small strain is applied)

P. Nazari, G. Hernandez-Sosa, U. Lemmer
Light Technology Institute
Karlsruhe Institute of Technology
Engesserstrasse 13, 76131 Karlsruhe, Germany
E-mail: pariya.nazari@kit.edu; uli.lemmer@kit.edu
P. Nazari, J. Zimmermann, C. Melzer, W. Kowalsky, G. Hernandez-Sosa, U. Lemmer
InnovationLab
Speyerer Str. 4, 69115 Heidelberg, Germany
W. Kowalsky
Institute of High Frequency Technology
Technical University of Braunschweig
Universitätsplatz 2, 38106 Braunschweig, Germany
J. Aghassi-Hagmann
Institute of Nanotechnology
Karlsruhe Institute of Technology
Hermann-von-Helmholtz-Platz 1, 76344 Eggenstein-Leopoldshafen, Germany
G. Hernandez-Sosa, U. Lemmer
Institute of Microstructure Technology
Karlsruhe Institute of Technology
Hermann-von-Helmholtz-Platz 1,
76344 Eggenstein-Leopoldshafen, Germany

The ORCID identification number(s) for the author(s) of this article can be found under https://doi.org/10.1002/adsr.202300189

DOI: 10.1002/adsr.202300189

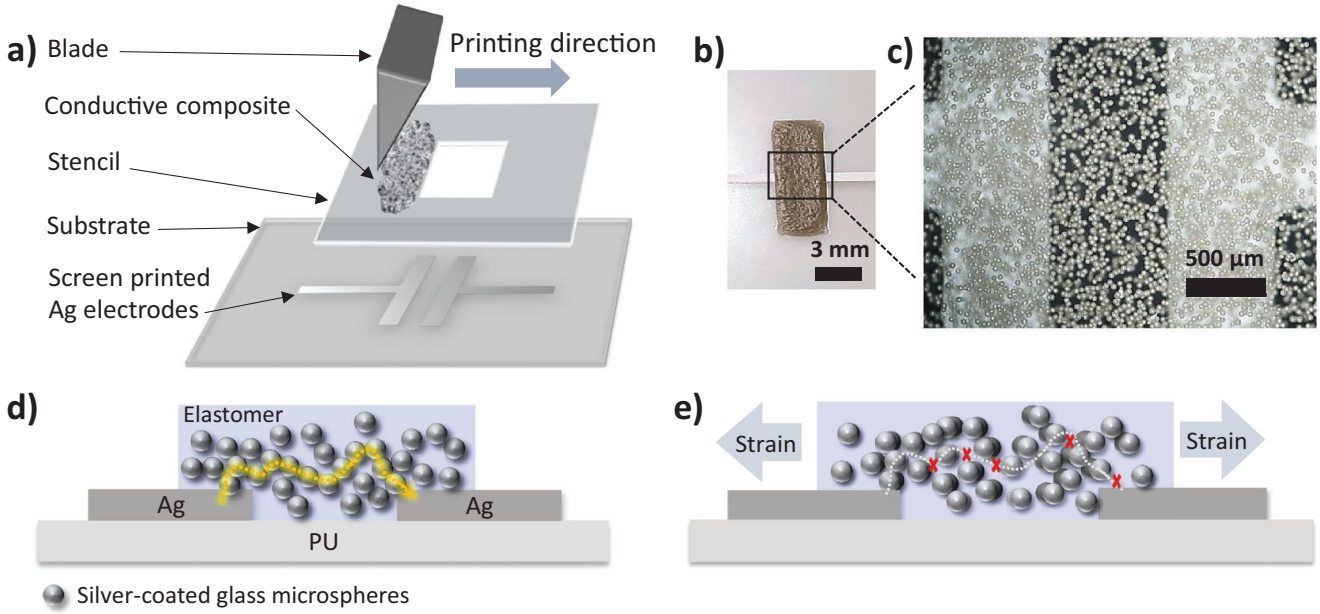

Figure 1. Fabrication method and structure of the stretchable strain sensor in this work. a) Before stencil printing of the sensing material, silver electrodes were screen printed onto the PU substrate. The substrate is brought into contact with the stencil and the blade is driven across the stencil surface. The paste passes through the stencil and is deposited onto and in between the electrodes. b) Photograph of the printed sensing material on the substrate (scale bar 3 mm). c) Optical microscope image of the printed material (scale bar 500 µm). d) Scheme of the cross-section of the stretchable sensor (not to scale). Above the percolation threshold, the conductive paths are formed by conductive microspheres. e) Tensile strain applied to the sensor causes displacement of the microspheres within the elastomer, disconnecting some of the conductive paths (schematic).

and high resolution (i.e., an easily distinguishable signal change when a small strain difference is applied) are more relevant than high stretchability.

Polydimethylsiloxane (PDMS) is one of the most widely used elastomers in composite sensors due to its flexibility and biocompatibility.[4–9] However, the fabrication process of PDMS-based sensors can be challenging mainly due to the spontaneous onset of the cross-linking process at room temperature.[10] Conductive materials used in composite sensors are mostly nanofillers (e.g., carbon black, graphene, or carbon nanotubes).[1,11] Nevertheless, to create a homogeneous mixture of nanoparticles and an elastomer, several additional time and energy-consuming dispersion steps are required to avoid their agglomeration.[12,13] A critical limiting factor of the sensitivity of nanofiller-based sensors, especially at small strain regimes (ϵ_{min} < 1%), is that the conductive paths are not significantly affected by the small strain, resulting in low sensitivity.

Huang et al. reported that polyvinylidene fluoride insulating nanospheres were grown inside wet-spun graphene-polyurethane microfibers, and a ten times higher sensitivity was achieved compared to using only the graphene network. They reported a minimum strain sensitivity of 0.01%.[14] Hwang et al. showed that a monolayer of gold-coated microspheres and PDMS elastomer matrix prepared by mechanical rubbing against dry microsphere powder provides a minimum detection limit of 0.3%.[15] Thus, an effective approach to achieving high sensitivity at small strain is to reduce the contact points between conductive fillers for example by using spherical particles. However, most of the literature has focused on strain sensing in larger ranges, while high-resolution small strain sensing and impact sensing using conductive microspheres fabricated by the printing method lag behind.[6–9,15–18]

Here, we employ conductive microspheres in an elastomer fabricated in a straightforward printing method for impact sensing and diaphragm strain sensing. Unlike nanoparticle fillers, our approach of using micron-scale conductive particles simplifies the fabrication process. As an elastomer, we investigate the low-cost ethylene vinyl acetate (EVA) as a preferable alternative to the commonly used and costly PDMS in terms of morphological and electromechanical properties. Furthermore, using EVA, with a special focus on small strain sensing, we evaluate the performance of the sensors. We successfully realized a highly linear response range from a small strain of 0.015% up to 6.7% and a stable electrical response after 1000 cycles of 0–1% strain. We demonstrate the EVA-microsphere-based sensor, for the first time, for high-resolution diaphragm expansion monitoring and impact sensing. Our findings demonstrate the potential of utilizing EVA-microsphere material, which provides highly sensitive strain sensors with enhanced electromechanical properties. These strain sensors can be mass-produced for use in a wide range of applications.

2. Results and Discussion

As a widely preferred technology for the fabrication of conformable electronics,[19,20] we use the stencil printing method (**Figure 1a**). In our work, a high-viscosity paste is prepared in one step by mixing an elastomer solution and silver-coated glass microspheres (core–shell). This paste is deposited directly on the screen-printed electrodes through a stencil mask on

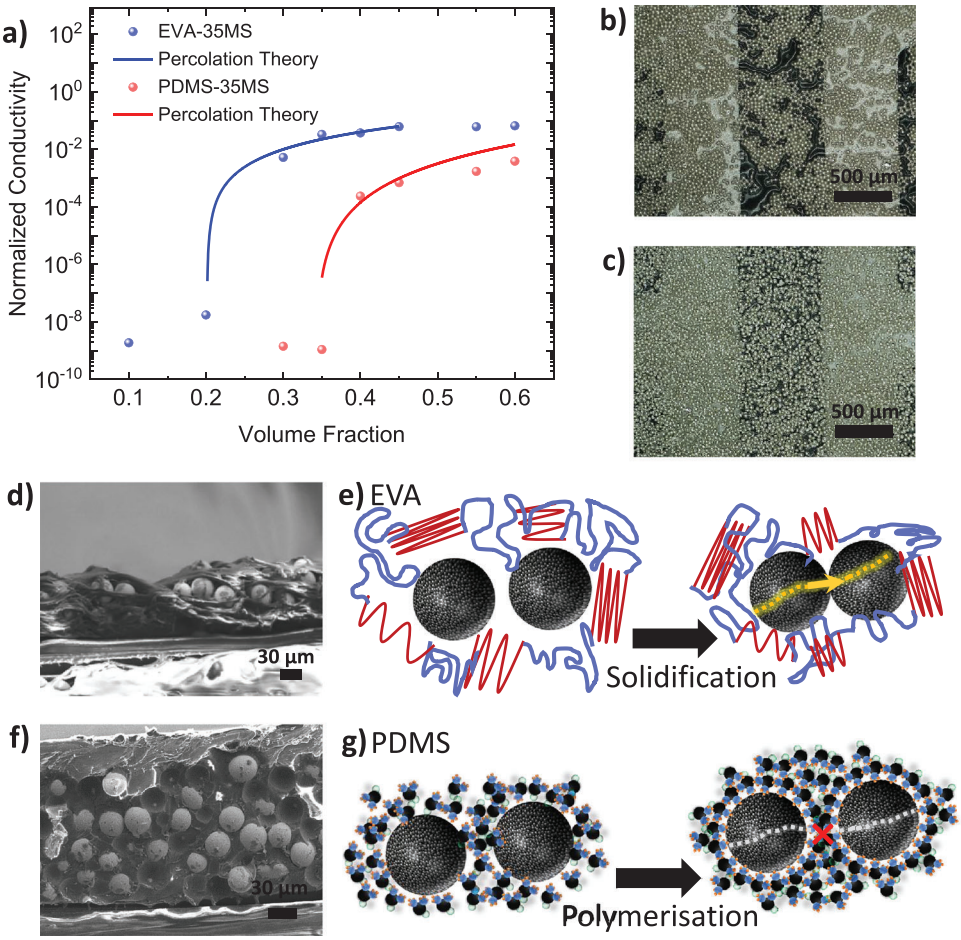

Figure 2. Comparison of the electrical percolation, and microstructure of EVA-35MS and PDMS-35MS composites (35 µm diameter microspheres are embedded in both elastomers). a) The experimental data of normalized conductivity as a function of different volume fractions are fitted to the percolation theory (Note S1, Supporting Information). The percolation threshold is 20% for the EVA-35MS composite and 34% for the PDMS-35MS composite, respectively. b) Optical microscope image of the EVA-35MS and c) PDMS-35MS. d) Cross-sectional SEM image of EVA-35MS. e) Schematic illustration of the interface formation mechanism between EVA and microspheres (schematic not to scale). f) Cross-sectional SEM image of PDMS-35MS. g) Schematic illustration of the proposed interface formation mechanism between PDMS and microspheres (schematic not to scale).

elastic polyurethane (PU) as a stretchable substrate. The simple ink preparation and printing method used here allows the scalable fabrication of stretchable sensors. As an elastomer matrix, we use either PDMS or EVA. To dissolve the EVA, we use anisole as a nontoxic solvent. After stencil printing of the sensing material onto the PU substrate, the deposited layer is cured or dried (see Experimental Section for details). Evaporation of the solvent in the printed material (or curing in the case of PDMS) results in the densification of the composite. Figure 1b,c shows a photograph and an optical microscope image of the composite-based printed sensor on the substrate, respectively. Based on the percolation theory,[21,22] above a critical volume ratio of conductive filler to the polymer, conductive paths start to form. Figure 1d shows a schematic of the cross-section of the stretchable strain sensor and how the microspheres form a conductive path between the electrodes. When an external strain is applied to the sensor (Figure 1e), the elastomer is stretched (while the microspheres are rigid). As a result, the microspheres are slightly displaced within the elastic matrix, causing partial interruption of the conductive paths, thus increasing the resistance of the sensor, i.e., piezoresistivity.

Since PDMS is widely chosen for fabricating piezoresistive composite sensors, we compare its electrical percolation threshold, filler interface morphology, and electromechanical response to strain with sensors fabricated using EVA. **Figure 2a** shows the experimentally measured conductivity of a composite comprising 35 µm microspheres in PDMS (abbreviated as PDMS-35MS) in red and a similar composite using EVA (EVA-35MS) in blue, fitted to the percolation theory (Kirkpatrick model) (Note S1, Supporting Information).[22] The percolation threshold for PDMS-35MS is estimated to be 0.34, while for EVA-35MS it is estimated to be 0.2. A relative decrease of 41% in the percolation threshold when EVA is used compared to PDMS indicates that conductive pathways are formed at a significantly lower volume fraction of microspheres when EVA is used as the elastomer. To investigate the reason for the difference in percolation threshold, we examine the morphology and the microstructure of the composites prepared with PDMS and those prepared with EVA

(both at 40 vol.%). As shown in the optical microscope image in Figure 2b, in EVA-35MS, clusters of agglomerated microspheres are formed.[23] In contrast, PDMS, shown in Figure 2c, produces a uniform distribution of microspheres with no visible agglomerates. A closer look at the microsphere-EVA interface in the cross-sectional SEM image in Figure 2d reveals that a loose layer of polymer is formed around the particles, facilitating the formation of a percolation network. The cross-sectional SEM of PDMS-35MS (Figure 2f) shows a densely packed polymer layer surrounds the microspheres, preventing effective agglomeration to create conductive pathways. In the schematics in Figure 2e,g, we illustrate a possible explanation for the observed differences. It is suggested that in the EVA matrix, the interface formation is mainly dominated by weak Van der Waals forces between the physically cross-linked chains and the silver coating. In PDMS, it is assumed that at the time of microsphere mixing, because the monomer chains are not fully polymerized, polymer-filler bond formation with silver precedes complete cross-linking. This explains why the microspheres in PDMS are more evenly distributed and separated from each other, leading to an overall lower conductivity (Figure 2a).

The electromechanical performance of the EVA-35MS and PDMS-35MS sensors is investigated through cyclic tensile strain and monitoring the resistance changes of the sensors during the test. **Figure** 3a displays a photograph of an EVA-35MS sensor including the screen-printed silver electrodes on the PU substrate for electromechanical testing. Tensile strain is applied in the longitudinal direction (Figure 3b). In Figure 3c,d the responses of the sensors as the relative changes in resistance as $\Delta R/R_0$ against an applied strain of 0.2% are shown. Here, R is the resistance at the applied strain ϵ, R_0 is the initial resistance of the sensor, and $\Delta R/R_0 = (R-R_0)/R_0$. To ensure a stable electromechanical response, we chose filler to elastomer volume fractions above the percolation thresholds of the composites (i.e., 35 vol.% for the EVA-35MS sensor, and 45 vol.% for the PDMS-35MS sensor). It is observed that in both cases the initial cycles result in a larger $\Delta R/R_0$ than the subsequent cycles. This effect seems to be much stronger for the PDMS-35MS sensor. As illustrated in Figure S1 (Supporting Information), the PDMS-35MS sensor shows a higher electromechanical hysteresis compared to EVA-35MS. As discussed elsewhere,[24,25] there is typically a strain-history-dependent response in piezoresistive elastomer-filler composites. This behavior is attributed to two well-known phenomena, i.e., the Payne effect and the Mullins stress softening effect,[26,27] which relate the observed gradual decrease in $\Delta R/R_0$ to the fracture of the glassy polymer layer around the filler, rupture of the filler-filler bond, and debonding of the filler-polymer chain. Furthermore, for both sensors, a shoulder pick appears in the relaxed state, as another type of electromechanical hysteresis (Figure 3c,d). However, for PDMS-35MS the magnitude of the shoulder peaks is observed to be larger than EVA-35MS. The increase in resistance with decreasing strain is called negative piezoresistivity,[28] a phenomenon that can be ascribed to the reconstruction of the disrupted conductive paths during the release of the strain.[29] The reason for stronger shoulder peaks in PDMS is probably due to the compact and glassy interface it forms with the fillers and slower molecular chain relaxation in its crystalline matrix.[10,30] It is noteworthy that PDMS requires a higher volume fraction of microspheres to achieve a repeatable sensor response. This may be another reason for the poor strain accommodation in PDMS. In EVA composite, during solvent evaporation, the polymer shrinks and wraps around the network of microspheres, compressing them to form agglomerated clusters with much less material in between, compared

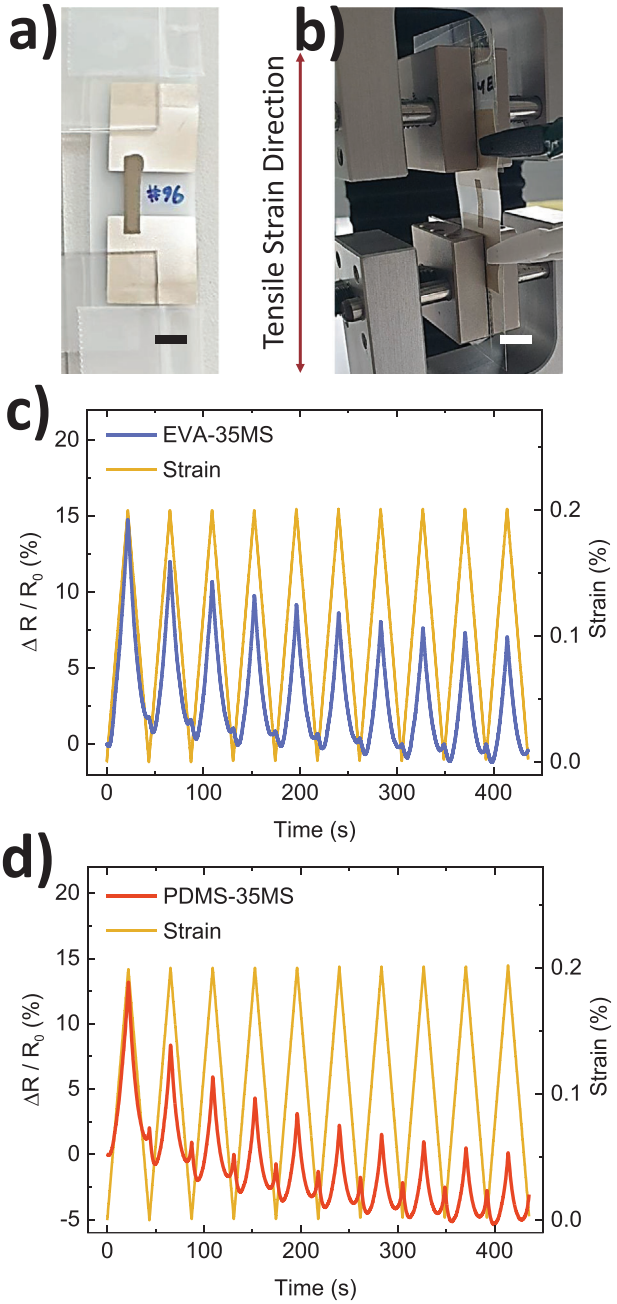

Figure 3. Comparison of dynamic cyclic tensile strain response of the EVA-35MS sensor with the PDMS-35MS sensor. 10 cycles of 0–0.2% strain-release are applied to both sensors at a strain rate of 0.5% min^{-1}. a) Photograph of the strain sensor prepared for electromechanical tensile strain tests with partially isolated electrodes from elongation applying clamps. b) Strain sensor under test instrument while the two-probe resistance measurement is performed using a source-measurement unit. c) Dynamic relative change of resistance of the EVA-35MS sensor. d) Dynamic relative change of resistance of the PDMS-35MS sensor.

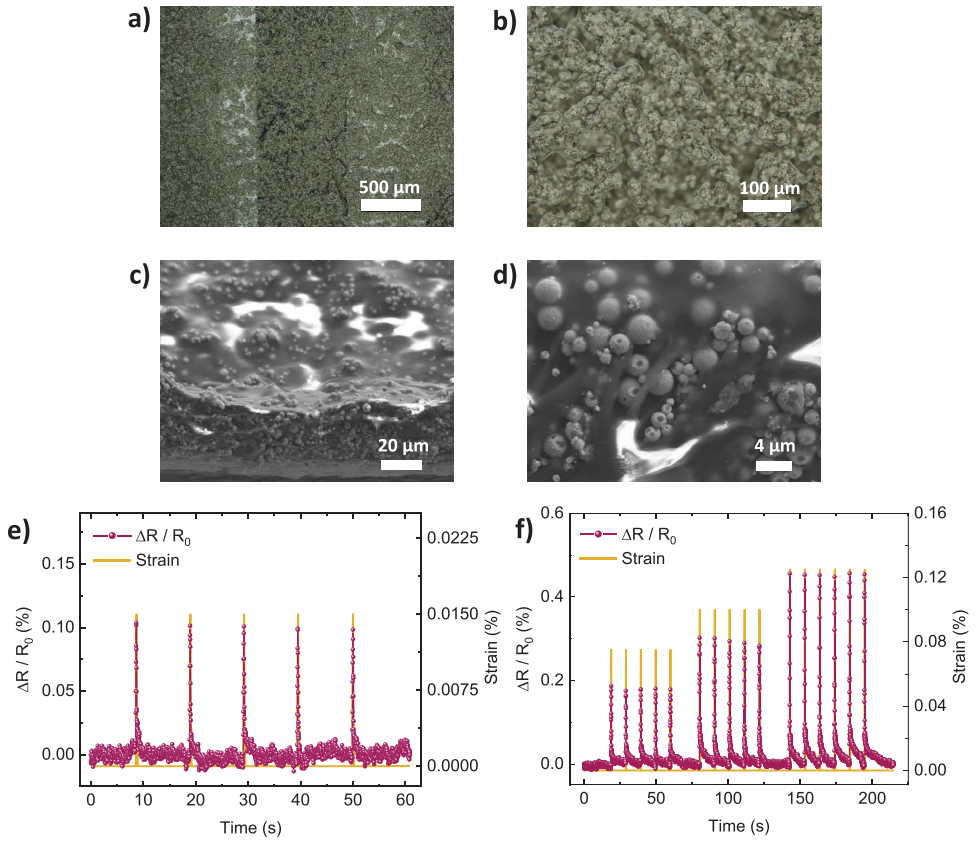

Figure 4. The microstructure of the EVA-4MS sensor (composed of EVA and 4 µm microspheres), and its minimum detection limit and resolution. a) and b) Optical microscope images of EVA-4MS composite, showing aggregated clusters of microspheres. c) and d) Cross-sectional SEM image of EVA-4MS. e) The relative resistance change of the EVA-4MS sensor showing a cyclic strain of 0.015% is easily detected. f) Response of the EVA-4MS sensor to the cyclic strain of 0.075%, 0.1%, and 0.125%, respectively, highlighting the resolution in detecting small strain differences.

to the PDMS matrix. Although there is only a weak interaction between EVA and microspheres, the microsphere leakage from the sensor is negligible, as evidenced from the durability data (see Figure S4, Supporting Information). Therefore, we prioritize EVA over PDMS for our sensors because it is a low-cost elastomer that effectively minimizes the percolation threshold and has lower electromechanical hysteresis. To realize higher stretchability, and less hysteresis we examine 4 µm diameter microspheres as conductive fillers. As shown in Figure S2 (Supporting Information), during cyclic strains larger than 0.2%, the shape of hysteresis is observed to be different in the two elastomers. In EVA, a negative piezoresistivity appears as the strain peaks and in PDMS a second peak in $\Delta R/R_0$ is observed as sensor is relaxed. The underlying reason behind these different behaviors is assumed to be the difference in the interaction of interfaces between the elastomers and the microspheres as well as the inherent difference between the mobility of the chains in PDMS and EVA.

EVA-35MS, as presented in Figure S3a (Supporting Information), reliably detects a strain of 0.01% ($\Delta L = 2$ µm). In this range, the response of the sensor ($\Delta R/R_0 = 0.41\%$) is highly repeatable and easily detectable. Figure S3b (Supporting Information) shows the ability to differentiate between small strain differences by applying three cyclic strains of 0.025%, 0.035%, and 0.055%. Here, a strain difference of 0.01% (0.035–0.025%) which is equivalent to a 2 µm difference in elongation, shows a +100% increase of $\Delta R/R_0$. This is interpreted as a significant resolution in distinguishing such small strain values. The electromechanical durability of EVA-35MS is examined under 600 cycles of 0–0.1% strain (Figure S4, Supporting Information). While EVA-35MS remains reliably responsive throughout 600 cycles, the $\Delta R/R_0$ values show fluctuations, from 0.4% to 0.8% in the 20–30th cycles to 0–0.7% in the 577–587th cycles. In **Figure** 4a,b, the optical microscope image of the printed composite with 4 µm microspheres is shown (EVA-4MS) indicating similar agglomerations as in EVA-35MS composite. The cross-sectional and top-view SEM images of the EVA-4MS, in Figure 4c,d respectively, reveal clusters of aggregated microspheres wrapped in EVA (similar to EVA-35MS). As shown in Figure 4e, the EVA-4MS sensor can reliably detect a strain of 0.015%. Figure 4f shows that a strain difference of +0.025% is easily detected by EVA-4MS with an increase of 67% in $\Delta R/R_0$. Previously, we reported a minimum detection limit of 0.005% in a freestanding microfiber sensor by using 4 µm microspheres.[31]

As presented in **Figure** 5a, the EVA-4MS sensor provides a repeatable and hysteresis-free signal for detecting cyclic strains of 0.5%, 1%, 2%, and 3%. The response time evaluation is depicted in Figure 5b when a 0.1% strain is applied. Our EVA-4MS

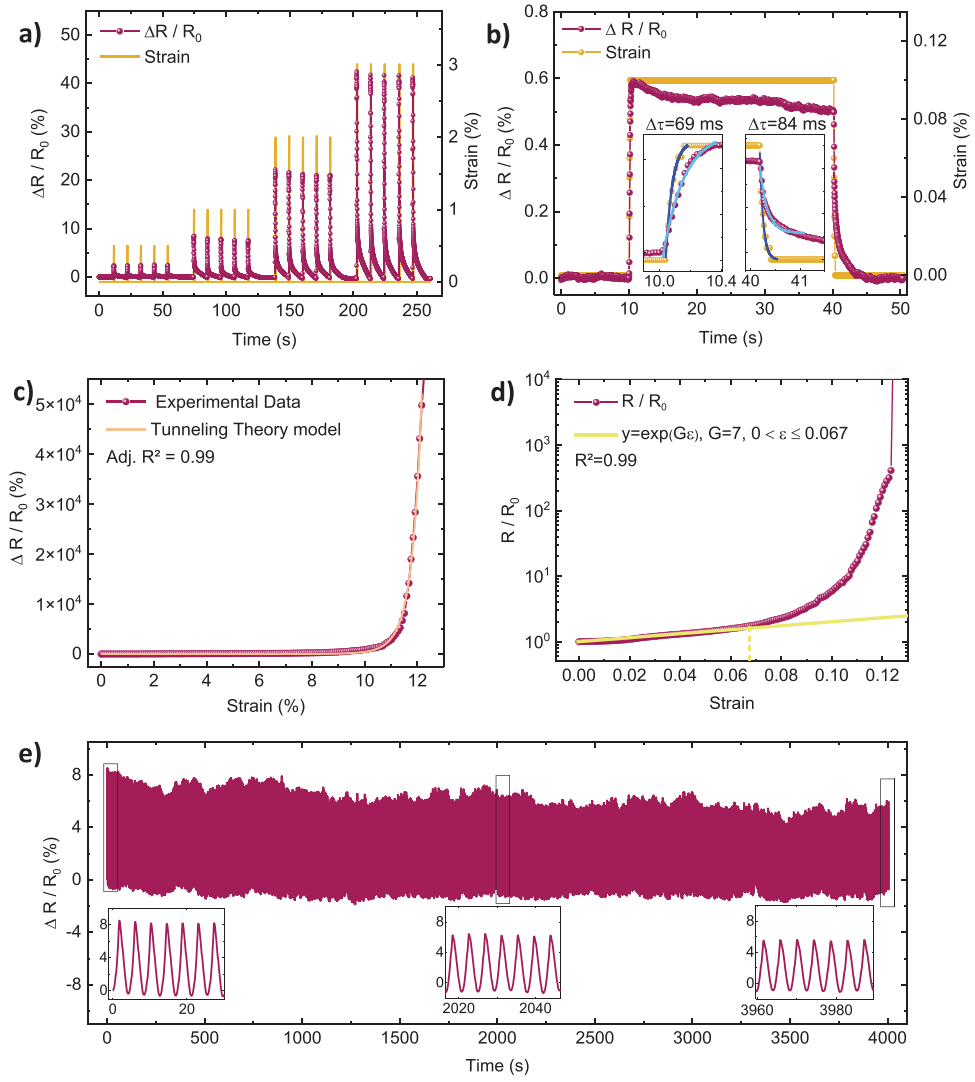

Figure 5. Sensing properties of the EVA-4MS sensor as the relative change of resistance of the sensor. a) Dynamic response of the sensor under a cyclic strain of 0.5%, 1%, 2%, and 3%. b) Response time evaluation as a strain of 0.1% is applied and released (Note S2, Supporting Information). Insets: zoomed in on the straining part (left) and releasing part (right) of the response. c) Response of the sensor in the conductive range as a function of applied strain and the fit to the experimental data based on the tunneling theory (Note S3 and Table S1, Supporting Information). d) Evaluation of strain sensitivity and the working factor as a function of applied strain. In the linear response range ($\epsilon \leq 6.7\%$), a strain sensitivity (G) of 7 is obtained by fitting the sensor data to Equation (2). The working factor is estimated to be 0.067. e) Electromechanical durability of the sensor response under 1000 consecutive cycles of 1% strain at a rate of 5% min^{-1}. The inset shows three temporal windows that are zoomed in during three spans of the test.

sensor $\Delta R/R_0$ signal transitions with an additional time constant (as compared to the actual strain) of 69 ms from the relaxed state to a strained state and relaxes with an additional time constant of 84 ms back. (Note S2, Supporting Information). These short response times are critical to provide real-time data in dynamic strain sensing applications.

As presented in Figure 5c, to explain the response mechanism of our sensor, we apply an increasing strain up to the point of electrical disconnection ($R_{\epsilon\,max} > 10^9$ Ohms). It is known that the piezoresistive response of a percolative network of conductive fillers embedded in an insulating polymer can be described by a tunneling theory approach.[22] As further details are explained in Note S3 (Supporting Information), based on this theory, the measured $\Delta R/R_0$ can be described based on the following equation

$$\frac{\Delta R}{R_0} = (1 + M\varepsilon)\exp\left[(P + FM)\,\varepsilon + Q\varepsilon^2 + T\varepsilon^3 + U\varepsilon^4\right] - 1 \qquad (1)$$

The experimentally measured response of the sensor, as shown in Figure 5c, agrees well with the tunneling model. To better illustrate the relationship between the response of the sensor in the electrically responsive range and the applied strain, $\Delta R/R_0$ as a function of applied strain is presented in Figure S5 (Supporting Information). The fitting parameters are given in Table S1 (Supporting Information). The strain sensitivity of a

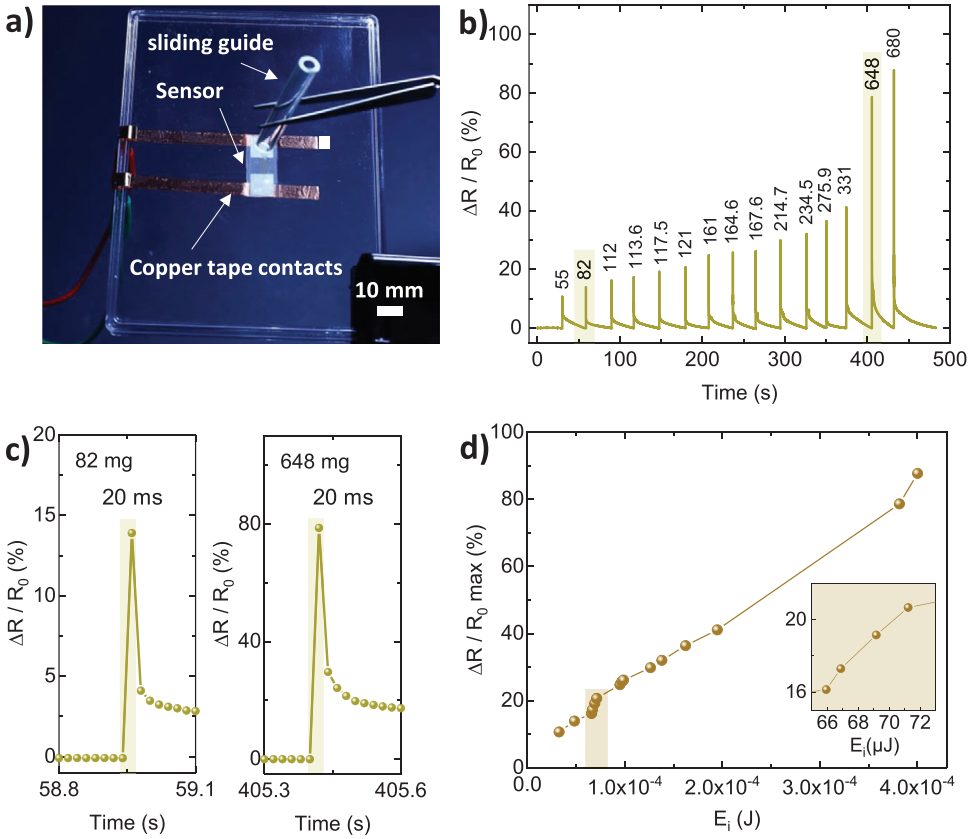

Figure 6. EVA-4MS sensor applied for impact sensing. a) Impact sensing test setup. During the test, while the resistance of the sensor is measured, small solid objects weighing 55–680 mg are dropped from a fixed height of 6 cm through the sliding guide at the center (back) of the sensor. b) Dynamic response of the sensor (shown as the relative change in resistance) to the impact produced by dropping the masses (the numbers in the graph are the weights of the solid objects in milligrams). c) Impact transient recorded by the sensor for two different objects. d) Response of the sensor as a function of exerted kinetic energy. Inset: The zoomed-in on the impact energy detected. The impact energy difference ΔE_i between the first two data points is less than 1 μJ.

stretchable sensor, i.e., the gauge factor (GF), can be formulated as $GF = \Delta R/R_0 \cdot 1/\Delta\epsilon$, a term applicable only to small strain ranges.[32] However, over the whole strain range the response of a stretchable sensor based on an elastomer-filler composite to applied strain is exponential (Equation 1), and a simplified equation to describe the strain sensitivity (G) can be defined as Equation (2).[33,34]

$$\frac{R}{R_0} = \exp(G\epsilon) \tag{2}$$

As shown in Figure 5d, based on fitting Equation (2) to the linear range of R/R_0 in a semilogarithmic plot, the estimated strain sensitivity of our sensor is 7. The threshold after which the resistance change becomes nonlinear (in the semilogarithmic plot), i.e., the working factor,[32,33] is estimated to be 0.067. We examine the durability of the strain sensor response by applying 1000 cycles of 1% strain. As the results are shown in Figure 5e, overall, our sensor provides highly reproducible $\Delta R/R_0$ throughout the test. The insets in Figure 5e present three time windows for cycling the sensor, showing a ≈6.5% increase for each cycle of strain. Comparing the first cycles to the middle cycles, a decrease in the measured $\Delta R/R_0$ values is observed. This is due to a typical stress-relaxation mechanism observed in filled elastomers under strain known as the Mullins effect.[25] As shown in Figure S6 (Supporting Information), starting from 5% onward, as strain is released a shoulder peak appears and it increases to values higher than the sensor response at the strain maximum. Therefore, the maximum detection range of the EVA-4MS sensor is estimated to be 6.7%.

2.1. Stretchable Strain Sensors Applications

Overall, the performance characteristics of our sensor meet the requirements of a variety of applications where reliable detection of small strains is the primary concern. As a demonstration of the applicability of our sensor, we examine the real-time response of the sensor to impact shocks as well as to a diaphragm expansion.

Impact sensing is commonly performed to determine the energy absorbed by a surface hit by an impact.[35,36] To exert a controllable impact and measure the impact energy with our sensor, we prepare a test setup in which small solid objects of different weights are dropped from a fixed height at the center of the sensor (**Figure 6a** and Experimental Section). $\Delta R/R_0$ of the sensor measured during the impacts is plotted in Figure 6b. A

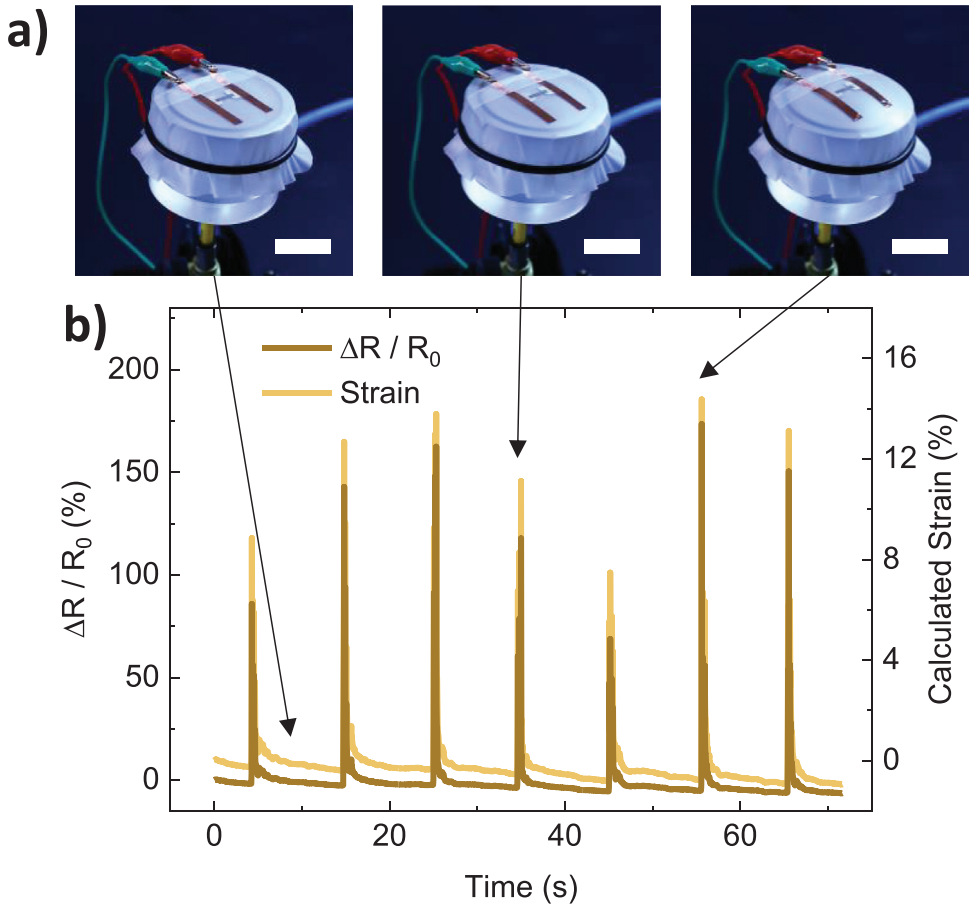

Figure 7. a) Photos from left to right: diaphragm in the relaxed state, inflated state, and increased inflation (scale bars 40 mm). b) Dynamic response of the EVA-4MS sensor applied to monitor the expansion of a stretchable diaphragm.

sharp increase in resistance at the time of impact and a subsequent gradual decrease is observed. This is a typical response shape for piezoresistive filler-polymer composites.[35,36] The impact time obtained by our sensor is remarkably short and is estimated to be ≈20 ms (Figure 6c) and independent of the mass of the dropped objects (55 mg < m < 680 mg). The energy absorbed by the surface, to which the sensor is attached, is calculated based on the assumption that the collision of the small objects with the fixed and solid surface is elastic. Thus, we assume the potential energy of the object m to be dropped at the height h equal to the kinetic energy during the impact on the sensor, i.e., impact energy $E_i = mgh$. As depicted in Figure 6d, there is a linear correlation between the maximum of $\Delta R/R0$ at the peak of the impact and the mass of the dropped object, or in other words, the impact energy. It is noteworthy that our sensor can easily resolve an impact energy difference as small as 0.942 μJ by a difference in $\Delta R/R_0$ of 1.2% (see inset in Figure 6d). This difference in impact energy is equivalent to distinguishing a Δm of 1.6 mg (113.6 mg − 112 mg) dropped from a height of 6 cm. This indicates the high-resolution capability of our sensor for impact-sensing. The lightest object we test weighs 55 mg and causes a maximum $\Delta R/R_0$ of 10.66% which amounts to an equivalent impact energy of $E_i = 32.61$ μJ, demonstrating the sensitivity of the sensor to such low-impact energies. The contact point concept by using conductive microspheres is assumed to provide such a fast response and high resolution. Overall, our findings on impact sensing using EVA-4MS sensor highlight the potential for future applications such as tactile sensing in robotic skins, or physiological parameters sensing such as pulse detection. As shown in Figure S7 and Table S2 (Supporting Information), the reported response time, strain detection resolution, and minimum detection limit presented in this work are superior compared to the piezoresistive strain sensors reported recently.

In addition to impact sensing, we demonstrate monitoring the expansion of a stretchable diaphragm with our sensor. For the expansion tests, we adhere our sensor to a deformable diaphragm (cut from the same PU substrate sheet). The diaphragm attached to the edges of a container is expanded at fixed intervals to different magnitudes by blowing compressed air (**Figure** 7a; Video S1, Supporting Information) and immediately releasing it. The dynamic response of the sensor as $\Delta R/R_0$ is plotted in Figure 7b. During the expansion and relaxation motion of the membrane, the resistance of the sensor increases and then recovers, respectively.

Expansion causes a sharp increase in resistance at the time of inflation, followed by a decrease when air is released. We estimate the corresponding strain experienced by our sensor during each cycle of expansion, based on the sensor response (R/R_0),

strain sensitivity of (G) 7, and $R/R_0 = \exp(G\epsilon)$. At the peak of diaphragm expansion in Figure 7a (right), our sensor detects a 14% strain with an increase in $\Delta R/R_0$ of 173%, and in Figure 7a (middle) it detects an 11% strain with an increase in $\Delta R/R_0$ of 118%. The results demonstrate the reversibility of the sensor response to strains greater than its working factor. These findings further highlight the applicability of our sensor for future studies on expandable surfaces, e.g. wearable sensors for diaphragm-breathing monitoring, and e-skins.

3. Conclusion

In summary, using a scalable method, we printed our sensor material on a stretchable substrate. The sensing element is a composite of conductive core-shell microspheres embedded in an elastomer. The electromechanical performance of the sensor against tensile strain is tested and it is successfully implemented for high-resolution impact energy sensing and diaphragm expansion monitoring. Our studies revealed that EVA has a lower electrical percolation threshold and less electromechanical hysteresis compared to PDMS. Using EVA as a promising alternative to PDMS, we further compared the performance of the sensor fabricated with 35 μm microspheres to that of 4 μm microspheres. The larger microsphere provides a lower detection limit (0.01%). The performance analysis of the sensor made with 4 μm microspheres demonstrated a high resolution, fast response time, high reproducibility, and a constant gauge factor of 7 up to a strain of 6.7% and electromechanical robustness to strain values larger than its working range. The promising dynamic response of our sensor enables high-resolution impact sensing and surface expansion monitoring for a variety of applications.

4. Experimental Section

Materials: Ethylene vinyl acetate copolymer resin with 40 wt.% vinyl acetate (ELVAX 40 W) was purchased from DuPont de Nemours, Inc. Polydimethylsiloxane elastomer (under the trade name of Sylgard 184) was purchased from Dow Corning Corporation as a two liquid component kit (part A as a base and part B as a curing agent). Conductive core-shell silver-coated soda lime glass microspheres (SLGMS-AG-3.3 1–7 μm – 10 g and SLGMS-AG-2.58 32–38 μm – 5 g) were purchased from Cospheric LLC. Elastic polyurethane (PU) substrate was purchased from Covestro Deutschland AG (PLATILON U 9122 150 NATURAL). Screen-printing silver paste was purchased from DuPont de Nemours, Inc. (DUPONT PE873). Anisole (anhydrous, 99.7%) was obtained by Sigma Aldrich. The materials were used as received.

Substrate Preparation: PU substrate with a thickness of 150 μm was cut into 40 cm × 60 cm pieces. As electrodes, screen-printed silver was mixed for 5 min manually and then screen-printed on the substrate. The deposited paste on the substrate was dried at 100 °C for 30 min. After drying the large substrate was cut into 30 mm × 50 mm pieces. The cut pieces were fixed on a glass slide using tape at the corners to prepare them for stencil printing of the sensing material in the next steps.

Preparation of the PDMS: PDMS mixtures were first prepared by mixing the base and the curing agent at the 10:1 mixing ratios by weight manually for 3 min. Then to remove the air bubbles formed during mixing, the mixture was degassed (3 pumping cycles under low-vacuum). The prepared PDMS was then used immediately for microsphere intermixing.

Preparation of the EVA Solution: The optimized EVA solution was prepared by mixing EVA copolymer resins having 40 wt.% vinyl acetate with anisole in a 1:4 weight ratio. This solution mixture was stirred at 55 °C for three hours to ensure the homogeneous dissolving of EVA in anisole. Then the prepared solution was kept at room temperature for 15 min to reach room temperature before microsphere filler intermixing.

Preparation of the Printing Paste: For the preparation of the printing paste, a solid powder of conductive core-shell microspheres was added to the prepared PDMS or EVA solution at room temperature by manual mixing for 30 s. The prepared paste was printed immediately after mixing.

Stencil Printing of the Paste: The stencil used for printing the sensing material was a polyethylene terephthalate (PET) foil having a rectangular mask at the center cut by laser, and a thickness of 170 μm. The substrate is brought in contact with the stencil and the blade is driven across the stencil surface. The paste passes through the stencil and is deposited on the electrodes. To allow for unstrained microsphere agglomerate formation, the printed layer is left untouched at room temperature for 1 hour. To ensure complete evaporation of the residual solvent, the EVA-MS sensors were dried at 40 °C under a 100 mbar vacuum. The PDMS-MS sensors (after room-temperature rest for 1 h) were placed in an oven at 80 °C for 12 h.

Preparation of the Stretchable Strain Sensors for Electromechanical Characterizations: With an active sensing length of 20 mm, contact electrodes at the two corners of the sensor were isolated using a 1 mm thick PET foil from the metal clamps of the strain-applying instrument. For the electrical resistance measurement, the contact electrodes are connected to two crocodile clamps of a source measure unit. The tensile strain is applied in the longitudinal direction of the sensor.

Characterizations of the Printed Strain Sensors: Field emission scanning electron microscopy (SEM) top-view and cross-sectional images of the sensors were taken with a ZEISS Supra 60VP scanning electron microscope. For the cross-sectional imaging, the printed sensors were cooled down using liquid nitrogen and broken. The micrograph images were taken using a Nikon Eclipse 80i microscope. For the electromechanical characterizations, the prepared sensors were strained by an Alluris Universal Test Instrument FMT-310BU with a 500 N force and displacement transducer head (FMT-310FUC5) with 0.1 N precision. For all electromechanical tests, the sensors were stretched at a fixed rate of 45% min^{-1}, unless otherwise specified. The electrical resistance measurements of sensors were carried out using a Keithley 2612B source measure unit, under a DC source voltage of 50 mV. 15 different small solid objects weighing 55–680 mg were dropped on the sensor from a height of 6 cm through the sliding guide that was fixed on top (at the back) of the sensor.

Preparation of the Sensor for the Impact Sensing Application: Printed sensors were used for impact sensing directly after they were dried and reached room temperature. A 12 cm long and 5 mm wide copper tape with conductive adhesive layer was attached to the screen-printed electrodes.

Impact Sensing Application: The sensor having copper tape attached to it, is adhered from the backside using a double-sided tape to a rigid 2 mm thick PET plate, which was held on top of a table using a vise swivel clamp. During the impact sensing, the electrical resistance of the sensor was measured in 2-probe mode using a Keithley 2612B source measure unit, under a DC source voltage of 50 mV. A slider guide, for the objects to be thrown, was fixed on the top and middle of the active sensing layer. 15 different small objects weighing 55 mg to 680 mg were dropped from a height of 6 cm at the back of the sensor.

Preparation of the Sensor and Surface Expansion Application: For the diaphragm, a 25 mm diameter circular sheet was cut from the same PU substrate sheet. The sensor was prepared as explained in the impact sensing application. The sensor was adhered to the diaphragm using double-sided tape, and the copper tapes were connected to the crocodile clamps. The diaphragm was fixated around a container, using an O-ring. Into the container pressurized air was pumped in and sucked out manually at fixed intervals.

Supporting Information

Supporting Information is available from the Wiley Online Library or from the author.

Acknowledgements

This work was financially supported by the 2HORISONS project (03INT606), a project funded by the Federal Ministry of Education and Research (BMBF). This research is also funded by the Deutsche Forschungsgemeinschaft (DFG, German Research Foundation) under Germany´s Excellence Strategy via the Excellence Cluster 3D Matter Made to Order (EXC-2082/1 – 390761711).

Conflict of Interest

The authors declare no conflict of interest.

Author Contributions

P.N. developed the idea and designed the sensors, designed the electromechanical experiments of this study, performed the strain tests, developed the impact sensing and diaphragm expansion monitoring ideas, and designed and prepared the impact sensing and diaphragm expansion setup. P.N., J.Z., and C.M. analyzed the SEM images. P.N., J.Z., C.M., G.H.S., and U.L. analyzed the results of electromechanical tests. P.N., C.M., J.A.H., and G.H.S. discussed the application experiments. P.N., J.A.H., G.H.S., and U.L. concluded the discussion of the application test results. U.L. supervised the project. All authors discussed the results and contributed to the manuscript writing.

Data Availability Statement

The data that support the findings of this study are available from the corresponding author upon reasonable request.

Keywords

Conductive microspheres, ethylene vinyl acetate, EVA, PDMS, piezoresistive strain sensors, polydimethylsiloxane, stretchable strain sensors

Received: November 28, 2023
Revised: February 5, 2024
Published online:

[1] Y. Luo, M. R. Abidian, J.-H. Ahn, D. Akinwande, A. M. Andrews, M. Antonietti, Z. Bao, M. Berggren, C. A. Berkey, C. J. Bettinger, J. Chen, P. Chen, W. Cheng, X. Cheng, S.-J. Choi, A. Chortos, C. Dagdeviren, R. H. Dauskardt, C. Di, M. D. Dickey, X. Duan, A. Facchetti, Z. Fan, Y. Fang, J. Feng, X. Feng, H. Gao, W. Gao, X. Gong, C. F. Guo, et al., *ACS Nano* **2023**, *17*, 5211.
[2] M. A. U. Khalid, S. H. Chang, *Compos. Struct.* **2022**, *284*, 115214.
[3] S. Kwag, Y. Ko, J.-Y. Jeon, D. Jang, M. Park, Y. Choi, J. Cho, H. Kim, *J. Mater. Chem. C* **2023**, *11*, 3796.
[4] H.-R. Lim, H. S. Kim, R. Qazi, Y.-T. Kwon, J.-W. Jeong, W.-H. Yeo, *Adv. Mater.* **2020**, *32*, 1901924.
[5] Y. Zheng, Y. Li, Z. Li, Y. Wang, K. Dai, G. Zheng, C. Liu, C. Shen, *Compos. Sci. Technol.* **2017**, *139*, 64.
[6] T. Li, J. Li, A. Zhong, F. Han, R. Sun, C.-P. Wong, F. Niu, G. Zhang, Y. Jin, *Sens. Actuat. A Phys.* **2020**, *306*, 111959.
[7] Z. Su, H. Chen, Y. Song, X. Cheng, X. Chen, H. Guo, L. Miao, H. Zhang, *Small* **2017**, *13*, 1702108.
[8] X. Liu, X. Liang, Z. Lin, Z. Lei, Y. Xiong, Y. Hu, P. Zhu, R. Sun, C.-P. Wong, *ACS Appl. Mater. Interfaces* **2020**, *12*, 42420.
[9] L. Su, M. Liang, J. Wang, X. Xin, Y. Jiao, C. Wang, Y. Zhang, Z. Yao, *Chem. Eng. J.* **2023**, *468*, 143564.
[10] T. Bardelli, C. Marano, F. Briatico Vangosa, *J. Appl. Polym. Sci.* **2021**, *138*, 51013.
[11] H. Souri, H. Banerjee, A. Jusufi, N. Radacsi, A. A. Stokes, I. Park, M. Sitti, M. Amjadi, *Adv. Intell. Syst.* **2020**, *2*, 2000039.
[12] V. Agarwal, Y. Fadil, A. Wan, N. Maslekar, B. N. Tran, R. A. Mat Noor, S. Bhattacharyya, J. Biazik, S. Lim, P. B. Zetterlund, *ACS Appl. Mater. Interfaces* **2021**, *13*, 18338.
[13] P. Costa, A. Maceiras, M. San Sebastián, C. García-Astrain, J. L. Vilas, S. Lanceros-Mendez, *J. Mater. Chem. C* **2018**, *6*, 10580.
[14] T. Huang, P. He, R. Wang, S. Yang, J. Sun, X. Xie, G. Ding, *Adv. Funct. Mater.* **2019**, *29*, 1903732.
[15] H. Hwang, Y. Kim, J.-H. Park, U. Jeong, *Adv. Funct. Mater.* **2020**, *30*, 1908514.
[16] Y. Zheng, Q. Jin, W. Chen, Y. Sun, Z. Wang, *J. Mater. Chem. C* **2019**, *7*, 8423.
[17] S. Liu, Y. Lin, Y. Wei, S. Chen, J. Zhu, L. Liu, *Compos. Sci. Technol.* **2017**, *146*, 110.
[18] K. Zhai, H. Wang, Q. Ding, Z. Wu, M. Ding, K. Tao, B.-R. Yang, X. Xie, C. Li, J. Wu, *Adv. Sci.* **2023**, *10*, 2205632.
[19] M. Wang, C. Ma, P. C. Uzabakiriho, X. Chen, Z. Chen, Y. Cheng, Z. Wang, G. Zhao, *ACS Nano* **2021**, *15*, 19364.
[20] A. Yoshida, Y.-F. Wang, T. Sekine, Y. Takeda, D. Kumaki, S. Tokito, *ACS Appl. Eng. Mater.* **2023**, *1*, 50.
[21] K. Shida, R. Sahara, M. N. Tripathi, H. Mizuseki, Y. Kawazoe, *Mater. Trans.* **2010**, *51*, 771.
[22] B. Agoudjil, L. Ibos, J. C. Majesté, Y. Candau, Y. P. Mamunya, *Compos. Part A Appl. Sci. Manuf.* **2008**, *39*, 342.
[23] Q.-H. Zhang, D.-J. Chen, *J. Mater. Sci.* **2004**, *39*, 1751.
[24] A. Georgopoulou, F. Clemens, *ACS Appl. Electron. Mater.* **2020**, *2*, 1826.
[25] C. S. Boland, *ACS Appl. Polym. Mater.* **2020**, *2*, 3474.
[26] D. Ponnamma, K. K. Sadasivuni, M. Strankowski, P. Moldenaers, S. Thomas, Y. Grohens, *RSC Adv.* **2013**, *3*, 16068.
[27] S. Merabia, P. Sotta, D. R. Long, *Macromolecules* **2008**, *41*, 8252.
[28] S. Biccai, C. S. Boland, D. P. O'Driscoll, A. Harvey, C. Gabbett, D. R. O'Suilleabhain, A. J. Griffin, Z. Li, R. J. Young, J. N. Coleman, *ACS Nano* **2019**, *13*, 6845.
[29] L. Duan, S. Fu, H. Deng, Q. Zhang, K. Wang, F. Chen, Q. Fu, *J. Mater. Chem. A* **2014**, *2*, 17085.
[30] H. Liu, Y. Li, K. Dai, G. Zheng, C. Liu, C. Shen, X. Yan, J. Guo, Z. Guo, *J. Mater. Chem. C* **2016**, *4*, 157.
[31] P. Nazari, R. Bäuerle, J. Zimmermann, C. Melzer, C. Schwab, A. Smith, W. Kowalsky, J. Aghassi-Hagmann, G. Hernandez-Sosa, U. Lemmer, *Adv. Mater.* **2023**, *35*, 2212189.
[32] C. S. Boland, *ACS Nano* **2019**, *13*, 13627.
[33] A. K. A. Aljarid, M. Dong, Y. Hu, C. Wei, J. P. Salvage, D. G. Papageorgiou, C. S. Boland, *Adv. Funct. Mater.* **2023**, *33*, 2303837.
[34] M. A. O'Mara, S. P. Ogilvie, M. J. Large, A. Amorim Graf, A. C. Sehnal, P. J. Lynch, J. P. Salvage, I. Jurewicz, A. A. K. King, A. B. Dalton, *Adv. Funct. Mater.* **2020**, *30*, 2002433.
[35] C. S. Boland, U. Khan, M. Binions, S. Barwich, J. B. Boland, D. Weaire, J. N. Coleman, *Nanoscale* **2018**, *10*, 5366.
[36] S. Y. Kim, B. G. Choi, W. K. Baek, S. H. Park, S. W. Park, J. W. Shin, I. Kang, *Smart Mater. Struct.* **2019**, *28*, 35025.